18TH WORLD CONFERENCE ON EARTHQUAKE ENGINEERING
WCEE2024
MILAN

MILAN, ITALY
30TH JUNE - 5TH JULY 2024

www.wcee2024.it

DAMAGE ASSESSMENT OF 2023 EARTHQUAKE BY VHR SATELLITE IMAGES IMPLEMENTING RESULTS OF SERAMAR PROJECT

N. Hadidian M.[1], J. Schwarz[2]

[1] Research Assistant in Earthquake Damage Analysis Center (EDAC),

Bauhaus Universität Weimar, Germany, nooshin.hadidian.moghaddam@uni-weimar.de

[2] Head of Earthquake Damage Analysis Center (EDAC), Bauhaus Universität Weimar,

schwarz@uni-weimar.de

Abstract: *In the aftermath of earthquakes, assessments using vertical satellite images predominantly focus on distinguishing between damaged and undamaged buildings in urban areas. This provides an immediate overview of the risk assessment post-event. Additionally, pre-event evaluations of building data inventories, including monitoring via instrumental tests considering factors like typology and vulnerability class, enable a more analytical approach to seismic risk forecasting. The qualification of seismic risk studies, based on set processes for monitoring building responses, was conducted over a decade (from 2004 to 2014) in Antakya, Turkey. This was part of the SERAMAR project, which stands for Seismic Risk Assessment and Mitigation in the Antakya-Maras-Region. The project was a collaborative effort between Turkish partners and the Earthquake Damage Analysis Center (EDAC) at Bauhaus Universität Weimar.*

The empirical and analytical risk assessments from this project, which serve as "pre-earthquake" estimations, are juxtaposed with post-earthquake damage evaluations derived from VHR satellite images captured shortly after the 2023 earthquake in Antakya, Turkey. Unlike other rapid damage overview services, this study's primary emphasis is on classifying damage grades in accordance with EMS-98 descriptions.

Sample areas, as well as the encompassed buildings, are selected based on multiple criteria and specifications, among which are zones of varying damage concentrations. The VHR satellite images used, captured by Worldview-2, have a resolution of 50 cm. This high resolution facilitates the distinct identification of observable damage grade indicators. To determine damage grades, a set of seven criteria is systematically applied, ensuring their alignment with the EMS-98 damage assessment standards through a criteria-based framework. This approach aids in building damage assessment at the building scale, especially given the absence of ground truth data. The overarching objective is to assess the alignment between damage grade distribution results from VHR satellite images and the prognostic scenarios of the SERAMAR project.

1. Introduction

Rapid response assessment following natural hazards has become pivotal, particularly when it revolves around damage grade assessment and risk analysis of physical assets in targeted areas. Despite its "rapid" nature, demanding quick execution, the results must be sufficiently accurate to proceed with the precise identification of hotspots and inform recovery actions. This is especially true when dealing with expansive

zones, such as those impacted by the devastating earthquakes that struck Turkey on 6 February 2023 — a topic that will be delved into further in this paper.

Furthermore, pre-disaster reconnaissance — identifying vulnerable areas, potential risk levels, and planning ground surveys for building data, soil types, fault lines, and more — can offer a comprehensive perspective on probable risk scenarios and the necessary mitigation actions.

An exemplary model of these preparatory and mitigation actions was presented in the SERAMAR project, titled "**Se**ismic **R**isk **A**ssessment and **M**itigation in the **A**ntakya-Maras **R**egion Based on Microzonation, Vulnerability, and Preparedness Studies" (EDAC, 2023). This project primarily focused on documenting exposed building stock, assessing vulnerability, and utilizing risk scenarios to enhance preparedness. Some outcomes from the project's executed scenarios are later compared with damage assessment results using multiple methodologies post the 2023 Earthquake in Turkey, as discussed by the authors in subsequent chapters.

In this devastating event, the USGS (2023) reported that the first shock, registering a magnitude of Mw=7.8, struck the Kahramanmaras-Pazarcik area near the northern border of Syria at 01:17:34 (UTC) on 6 February, originating at a depth of 10 km. Approximately 9 hours later, at 10:24:48 UTC, a second shock with a magnitude of Mw=7.5 hit the Elbistan zone, with its epicenter at a depth of 7.4 km.

Additionally, Çetin and Ilgaç (2023) noted that these tremors caused extensive destruction and loss across eleven provinces in Turkey, namely Kahramanmaraş, Adıyaman, Hatay, Osmaniye, Gaziantep, Kilis, Şanlıurfa, Diyarbakır, Malatya, Adana, and Elazığ.

Of the eleven provinces mentioned above, the city of Antakya in Hatay Province has been selected for a damage assessment study. This study employs rapid change detection methods and utilizes the EMS-98 - Grünthal *et al.* (1998)- systematic criteria-based framework with VHR satellite images. Further insights were derived from the rapid damage assessment conducted by Copernicus (2023), which served as a comparative benchmark for the level and location of detected damage areas in Antakya. Notably, Copernicus employed the same type and quality of satellite imagery.

In subsequent sections, the results of the building stock survey from Google Street Map (2023) for selected Regions of Interest (RoIs) in Antakya will be presented, formatted similarly to the SERAMAR project, facilitating an evaluation of alignment. Additionally, the distribution of damage grades for buildings within each RoI will be assessed against suitable shaking scenarios for damage prognosis, factoring in the corresponding intensity of shaking.

2. Data acquisition

For the implementation of the EMS-98 systematic criteria-based framework method, two VHR (Very High Resolution) Worldview-2 satellite images, both pre- and post-event, were procured by EDAC with the following specifications:

1. The pre-event image, taken on 22 December 2022, boasts a spatial resolution of 50 cm, has zero cloud cover, is 4-band pansharpened, and was taken at a 17.5º off-nadir angle.
2. The post-event image, captured on 8 February 2023 (2 days after the earthquakes), has a spatial resolution of 50 cm, 4% cloud cover, is 4-band pansharpened, and was taken at a 40.2° off-nadir angle.

Both images have been orthorectified and enhanced by the selling company. Figure 1 provides a visual comparison of the pre- and post-event images.

In the application of rapid change detection methods and for comparing the results, various tools such as QGIS, ERDAS-IMAGINE, and MATLAB were employed. These tools were chosen based on their capabilities with different mathematical algorithms.

In the effort to compare results with the outcomes of the SERAMAR project, a visual comparison with figures from published papers related to the project was utilized due to the lack of access to detailed building stock surveys. Additionally, to define district borders for the city of Antakya, the district zones map from Schwarz *et al.* (2008) was manually overlaid onto the VHR satellite images. This approach assisted in pinpointing the location, boundaries, and the buildings within each district.

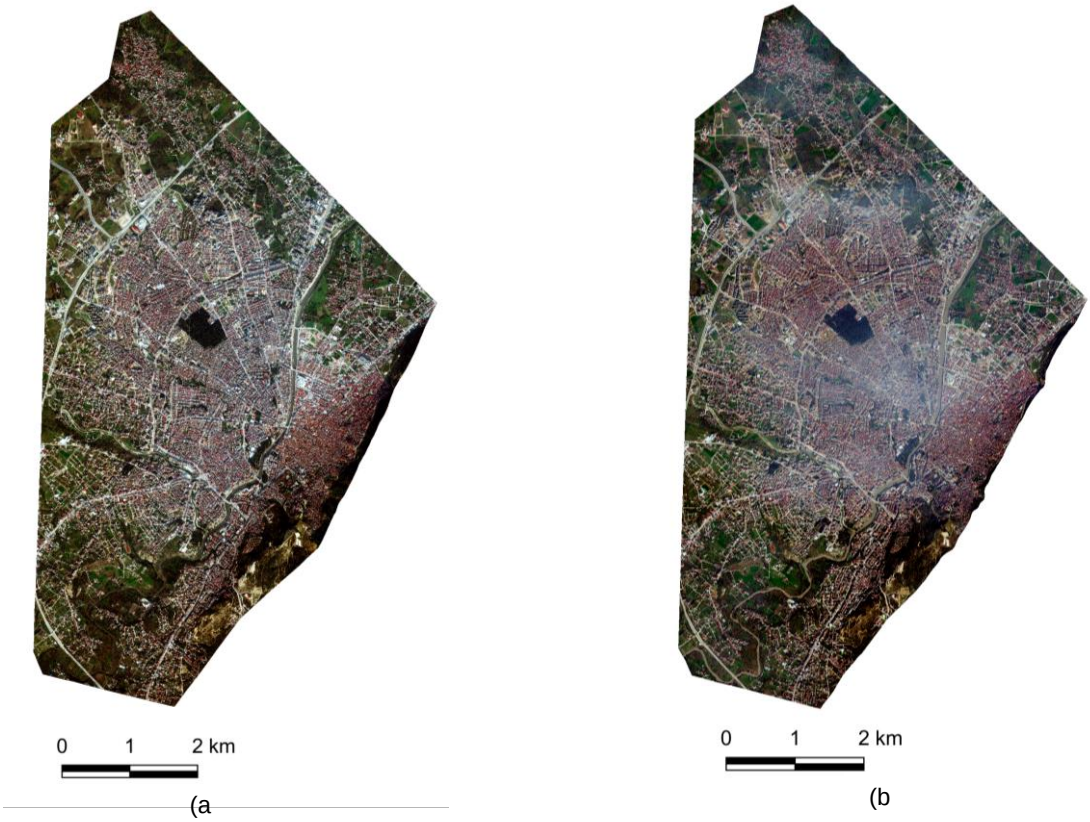

Figure 1. VHR Images of Antakya -purchased from Apollomaping- a) Pre-event and b) Post-event images

For the evaluation of rapid damage assessment by Copernicus (2023) in Antakya, emphasis was placed on the published figures for the old region of the city. It should be noted that the rapid estimation from Copernicus employed VHR satellite images with identical spatial resolutions to those provided by EDAC. This matching in image quality underscores the importance of the subsequent comparative analysis."

3. Methodologies

3.1. Rapid Response Assessment

This step includes five methods based on their different definitions in mathematical grounds which are done on temporal VHR satellite images. These approaches are explained as below:

1. CVA-Method: Change Vector Analysis (CVA) is used mostly in Remote Sensing to determine and quantify changes by comparing multi-temporal datasets like pre- and post-event images for a natural event. It provides information on both the magnitude and the direction of changes. This method is examined using MATLAB scripts by the main author. The results are classified based on defined patches with relevant average RGB values based on the scaled legend of colors.
2. ADCD-Method: The Additive Discriminant Change Detection (ADCD) method is an approach to quantify and identify changes between multi-temporal remote sensing datasets at different points. Its function accentuates the distinctions between these images while minimizing the variance of areas that haven't experienced change. After the formation of discriminant function, a threshold is applied to classify pixels into 'changed' or 'unchanged' categories. Pixels with discriminant values above this threshold are usually considered as 'changed'. The amount of changes can be determined by training the data using ground survey data or another sources.
3. SDCD-Method: The Subtractive Discriminant Change Detection (SDCD) method is similar in principle to ADCD approach. While both methods aim to discern changes in multi-temporal datasets, ADCD relies on a weighted combination (addition) of images, and SDCD focuses on the direct difference (subtraction) between images.
4. Combined Discriminant-Method: The Combined Discriminant Function for change detection integrates both additive and subtractive strategies to formulate a discriminant function. By leveraging the strengths

of both methods, this function aims to amplify the discernibility between regions that have undergone change and those that have remained static.

5. Image Difference-Method: In the Image Difference method, corresponding pixels from two multi-spectral images (usually taken at different times) are subtracted from one another to produce a difference image. Changes between the two dates will manifest as non-zero values in the difference image, while areas without any change will have a value of zero.

The last four methods were implemented automatically using ERDAS-IMAGINE software, and their results were processed in QGIS based on the outcomes from the EMS-98 systematic criteria-based framework evaluation on VHR satellite images. More details about this process will be discussed in the next section. The concept and preliminary results from the employed methodologies are represented in Table 1, Table 2 and Table 3.

Table 1.The concept of Change Vector Analysis method on VHR images and its result

Methodology	Definition/Concept	Result on VHR Imgs.
CVA	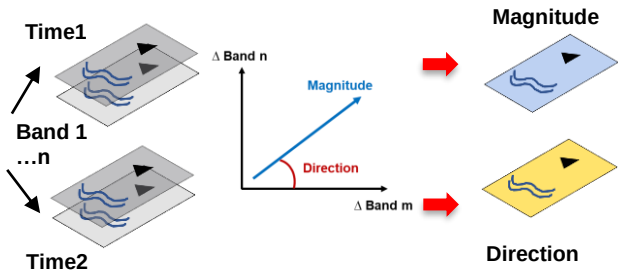	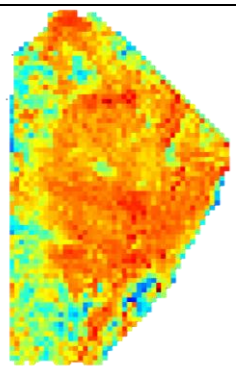

Table 2. The results of ADCD and SDCD for rapid response assessment

Methodology: ADCD	**Methodology:** SDCD
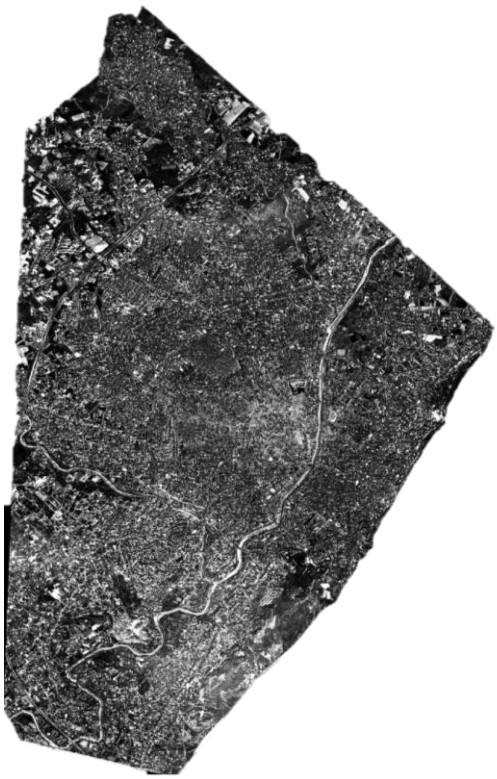	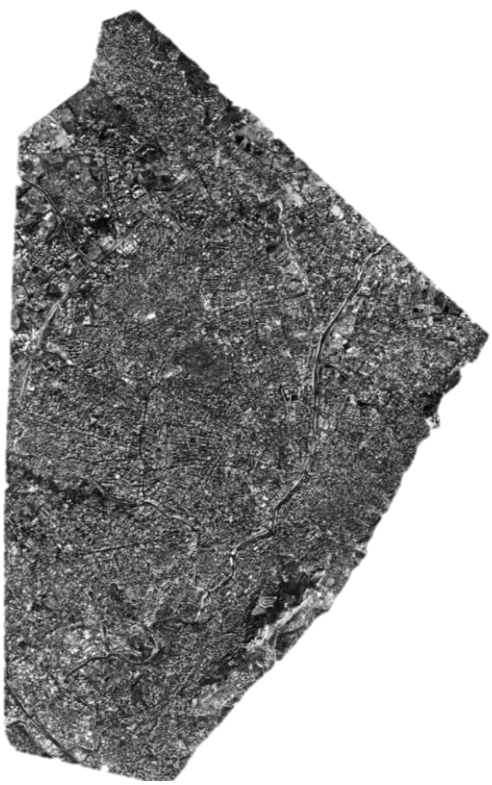

Table 3. The results Combined Discriminant and Image Difference for rapid response assessment

<table>
<tr><td colspan="2">Methodology: Combined Discriminant</td><td>Methodology: Image Difference</td></tr>
<tr><td colspan="2"> 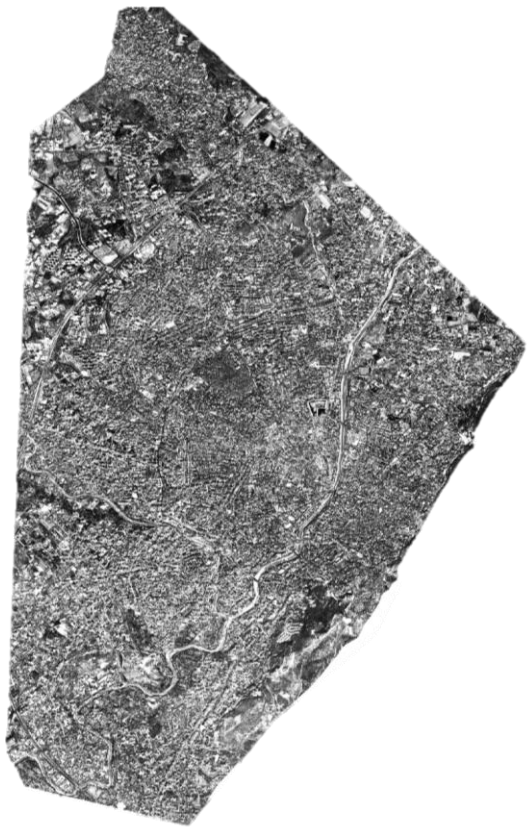 </td><td> 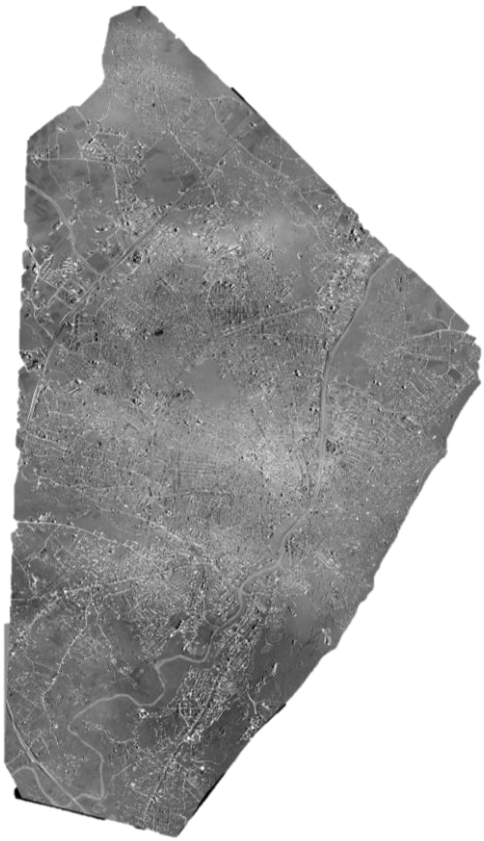 </td></tr>
<tr><td>Method</td><td>Equation</td><td>Parameters</td></tr>
<tr><td>ADCD</td><td>$D(X) = a \times X_{t1} + b \times X_{t2}$</td><td rowspan="4">$D(X)$ =Change Detection function
X_{t1}= Pixel value at time t1
X_{t2}= Pixel value at time t2
a, b = Weighted coefficients (ADCD)
W = Weighting Matrix (SDCD)
$M = ||D(X)||$, Magnitude of change (SDCD)
$A, B\ and\ C =$ = Weighting Matrices (Combined Discriminant)</td></tr>
<tr><td>SDCD</td><td>$D(X) = W \times (X_{t1} - X_{t2})$</td></tr>
<tr><td>Combined Discriminant</td><td>$D(X) = A \times X_{t1} + B \times X_{t2} + C \times (X_{t2} - X_{t1})$</td></tr>
<tr><td>Image Difference</td><td>$D(X) = X_{t1} - X_{t2}$</td></tr>
</table>

3.2. EMS-98 systematic criteria-based framework method

Building-by-building data evaluation offers a comprehensive inventory in the ground survey procedure for risk assessment, ensuring a high certainty level and a harmonized framework for data interpretation. In situations where a ground survey inventory is unavailable, especially following natural hazards, geospatial datasets become indispensable. They serve not only for rapid response assessment, as described in the previous section, but also for evaluating damage at the building scale. To address this need, this paper's response author, developed the EMS-98 systematic criteria-based framework. This method aims to overcome the challenges of certainty level using vertical VHR satellite images and to harmonize damage level definitions. Its design ensures high compatibility with EMS-98 scales, offering a framework closely aligned with ground survey damage assessments conducted via visual inspection. Case studies by Hadidian and Schwarz exemplify the application of this method. They investigated multi-natural hazard scenarios in Palu, Indonesia (2022) and flood damage in Germany (2023), demonstrating impressive accuracy levels in both cases. The core of this

Table 4. Definition of criteria for damage assessment in visual interpretation method on VHR satellite images for mono- and multi- natural hazard condition (Hadidian & Schwarz,2022)

No.	Criterion	Example	EQ (Mono Hazard)	EQ + Tsunami (Multi-Hazard)
1	Texture		√	√
2	Color		-	√
3	Shadow		√	√
4	Shape/Orientation		√	√
5	Surrounding		√	√
6	Neighborhood		-	√
7	Usage		-	√

methodology comprises seven criteria, tested on various remote sensing images, such as satellite and aerial images, spanning a broad spectrum of spatial resolutions for both HR and VHR vertical images and diverse off-nadir angles. Table 4 presents a concise overview of the criteria integral to this method.

4. Data analysis and results

To compare the damage grade distribution across various methods, five Regions of Interest (RoIs) were selected based on the location of district borders defined by Schwarz *et al.* (2008). In the first step, the shape-file of these districts was overlaid onto the colored patch-formed result of the CVA method (see Table 1), allowing for the evaluation of the mean damage grade for each district which is shown in Figure 2. The sample district and included buildings were selected based on their color position within the color spectrum legend produced by the CVA method and their qualitative value in Figure 2.

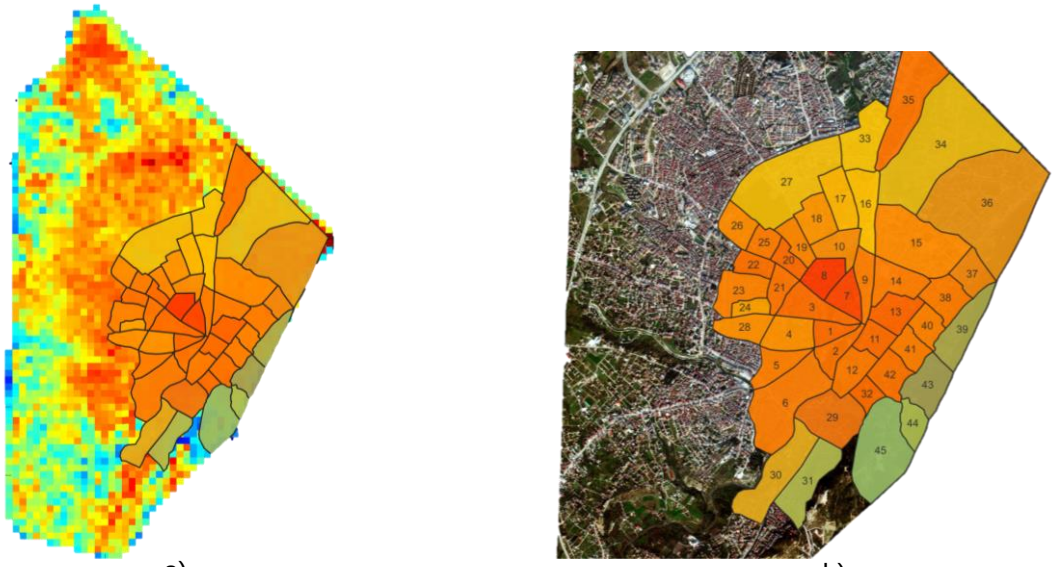

a) b)

Legend	< 0.4	0.4 - 0.5	0.5 - 0.6	0.6 - 0.7	0.7- 0.8	0.8 - 0.85	0.85 <
D_f	*No DG*	*Less DG*	*Few DG*	*Moderate DG*	*High DG*	*Very high DG*	*Total DG*

*Description:
First row shows the quantitative of changes in CVA method with relevant color range for defined dimension of each patch. The conversion of CVA values to qualitative damage classes are done based on combination of trained cases using CVA and visual inspection methods.

Figure 2. a) Mean Damage Grade of districts using colored patch images using CVA, b) Mean Damage Grade of districts overlapped on VHR images (enlarged figure) with related legend

Table 5. Characteristics of each district and surveyed building stock in pre- and post-earthquake phases using visual inspection approach on 3D Google Street Map and VHR satellite images

Dist.	Buildings			
	No. Story	**Structural Type**	**VC**	**DG**
1	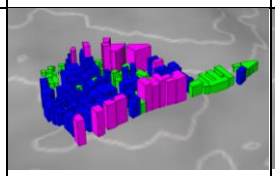	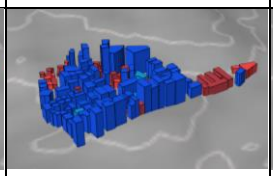	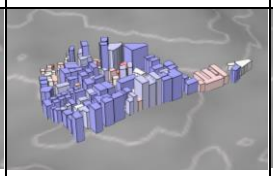	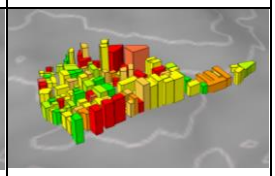
3	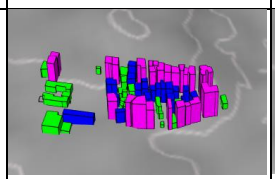	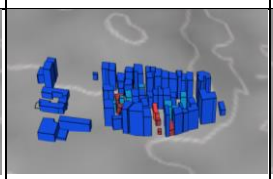	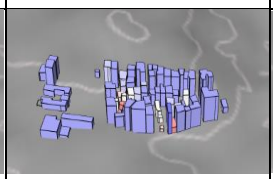	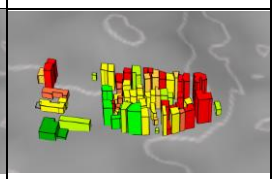
7	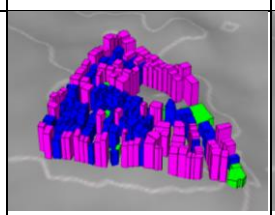	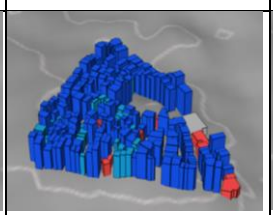	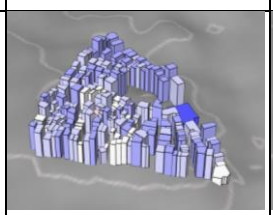	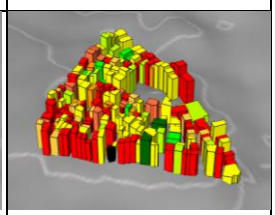
13	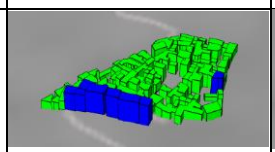	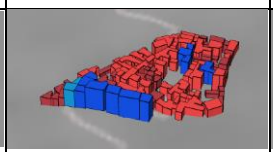	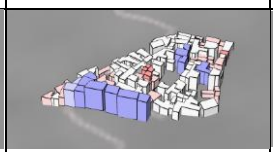	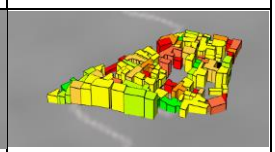
16	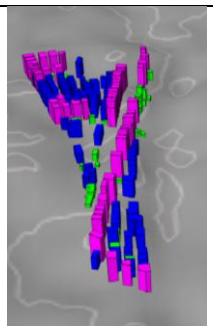	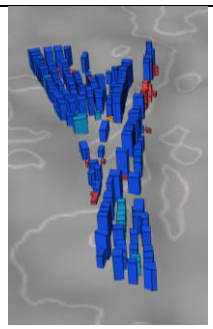	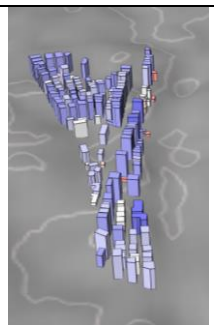	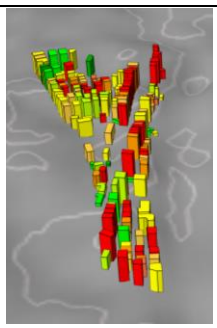

*Description: D(i) shows the number of each district.

Legends:

No. Story: Colors are based on Schwarz et.al,2009, SERAMAR Project

No. Story	n≤3	3<n≤6	6<n
Color			

Structural Type: Colors are based on Schwarz *et al.* (2021)

Str.Type	MUR	MUR/RC_L_ERD	RC_L_ERD	RC_M_ERD	Steel
Color					

Vulnerability Class

VC	A	AB	B	BC	C	CD	D	DE	E	EF	F
Color											

Damage Grade

DG	0	0-1	1	1-2	2	2-3	3	3-4	4	4-5	5
Color											

Table 6.Visual comparison of Damage Grade distribution in selected districts between rapid response and EMS-98 criteria-based framework methods

Dist.	DG distribution				
	M1: ADCD	**M2: SDCD**	**M3: Combined Discriminant**	**M4: Image Difference**	**EMS-98 criteria-based**
1	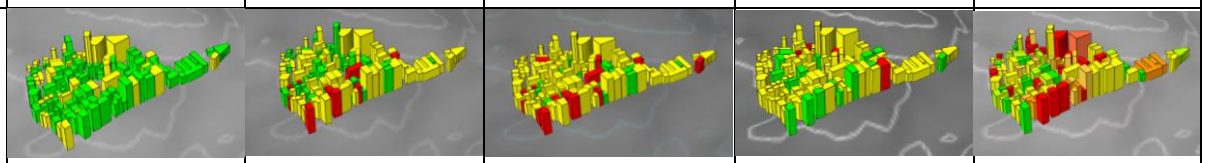				
3	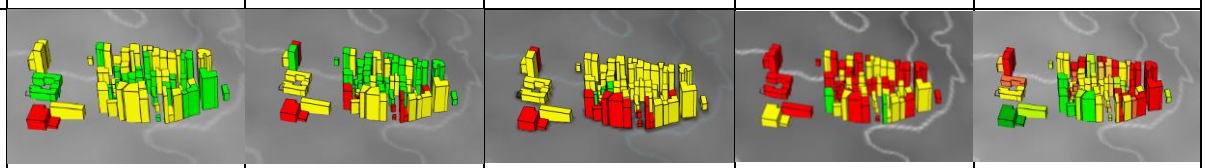				
7	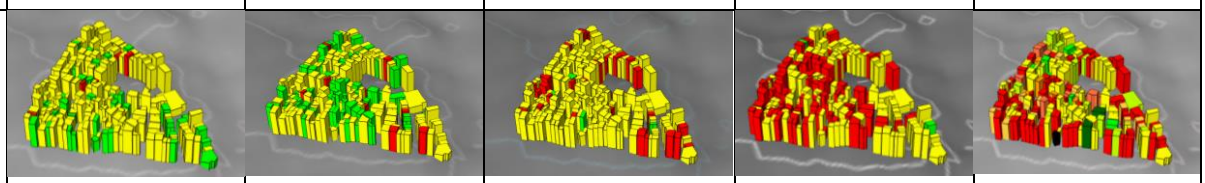				
13	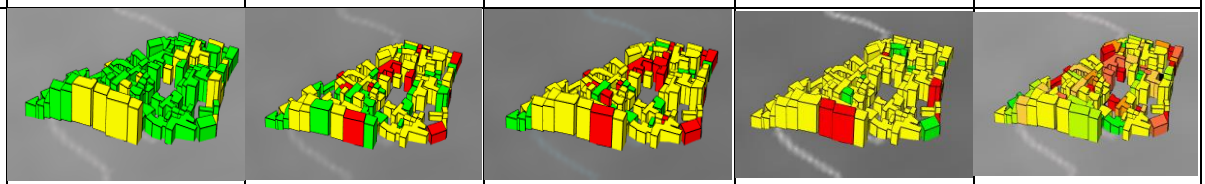				
16	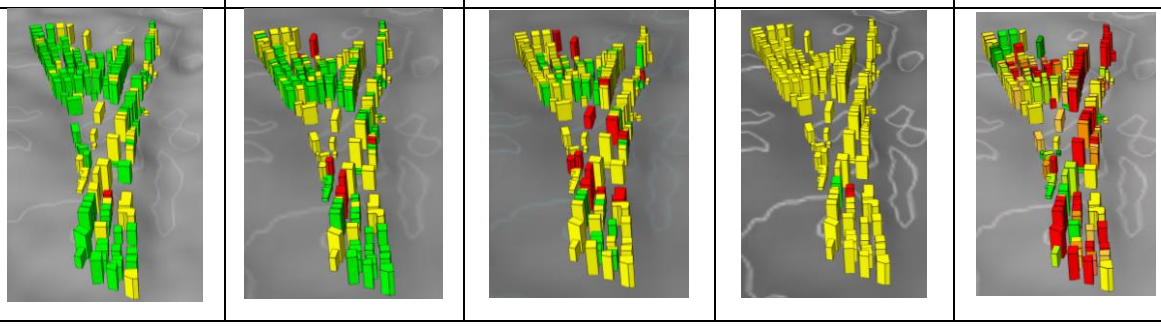				

*Description:

DG-Rapid Response			
DG-Qualitative	No-Low	Moderate-High	Very High-Total
DG-EMS-98	0 ≤ Di ≤ 2	2 < Di < 4	4 ≤ Di ≤5

The characteristics of the selected districts and the surveyed building stock in the pre- and post-earthquake phases, using visual inspection approach on 3D Google Street Map and VHR temporal satellite images, are detailed in Table 5.

Damage grade assessments utilizing the EMS-98 criteria-based framework serve as a reference for comparison with rapid response analysis methods (see Table 2 and Table 3). Analysis of outputs from these rapid response techniques involved post-processing of associated images to determine the percentage change in buildings. To ensure precise categorization of changes in buildings, three qualitative categories were employed. These classes are designed to align with EMS-98-based quantitative scales, facilitating subsequent comparisons. Table 6 presents the results of building damage distribution using rapid response methods (exclude CVA) and their visual comparison to the EMS-98 criteria-based framework approach.

Table 7. Bland-Altman plots to compare the difference of results for each rapid response method with EMS-98 criteria-based approach in selected districts

Dataset 2	Bland-Altman plots for District				
	1	3	7	13	16
M1-ADCD	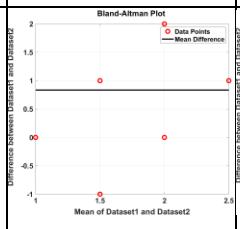	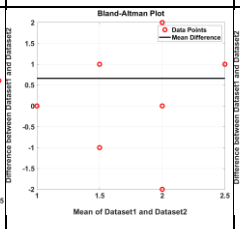	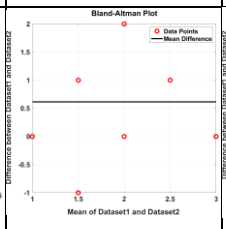	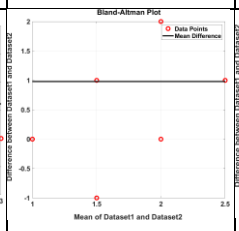	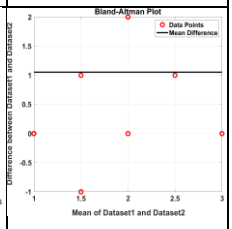
M2-SDCD	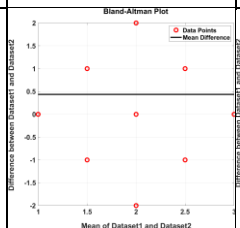	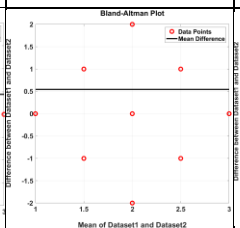	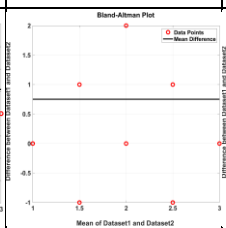	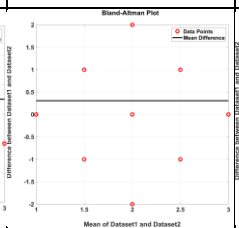	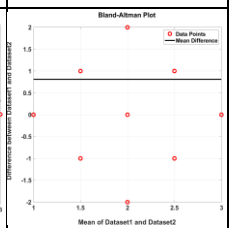
M3-Combined Discri-minant	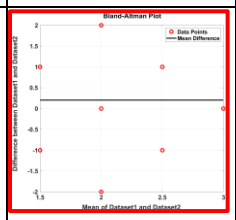	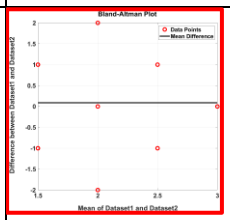	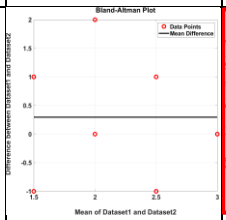	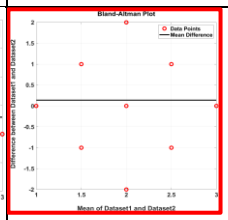	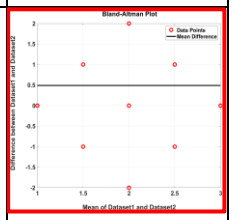
M4-Image Difference	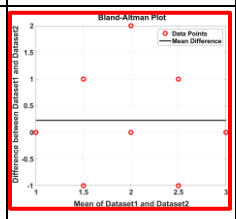	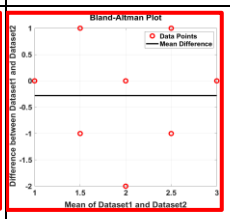	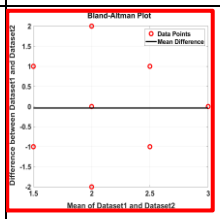	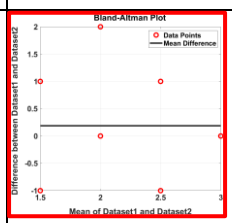	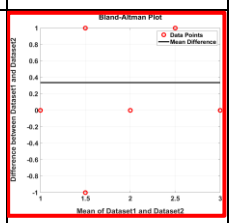
Best fit	M3 & M4	M3 & M4	M4	M3 & M4	M3 & M4

To assess the agreement between the results from rapid response methods and the EMS-98 criteria-based framework, a method of Bland-Altman plot is employed. This method aims to detect any systematic differences between measurements, assuming a normal distribution. The plot indicates whether variability remains consistent across measurement ranges or if proportional differences exist (e.g., where differences are more pronounced at higher measurement values). Table 7 displays the Bland-Altman plot comparing 'Dataset1=EMS-98 criteria-based' with 'Dataset 2=Rapid response method-I' for each selected district and related conclusions. To interpret the Bland-Altman plots following steps have been considered:

1. Mean Difference line: The closer the mean difference is to zero, the better the agreement between the two methods.
2. Scatter of Data Points: Most clustered Data Points (Red points in graph) around mean difference line suggests more consistency between measurements in two methods.

Table 7 reveals that, across all districts, the best-fit measurements for rapid response assessment on the introduced temporal VHR satellite images come from the combined discriminant and image difference methods as highlighted with red frames. The evaluation of CVA results, based on visual inspection through the EMS-98 criteria-based framework, was conducted for the entire district by comparing the mean damage grades of CVA patches and the included buildings. The results of this comparison are shown in Table 8 for three selected districts based on the level of mean damage grade (see Figure 2). The outcomes demonstrate a strong agreement between CVA and the visual inspection method, despite the high nadir-off angle of the post VHR image.

Table 8. Comparison of mean damage grade between CVA and EMS-98 criteria-based framework methods on selected districts

District	Mean DG, buildings		Mean DG, patches		Difference (Δ)
1	Moderate to High		High		Less to few
7	High		High to Very High		Less to few
16*	High		Moderate to High		Less to few
* Some parts of District-16 are covered with vegetation, which experienced very minimal changes in the CVA method. As a result, the mean damage grade of these patches falls within the lighter range of spectral colors.					

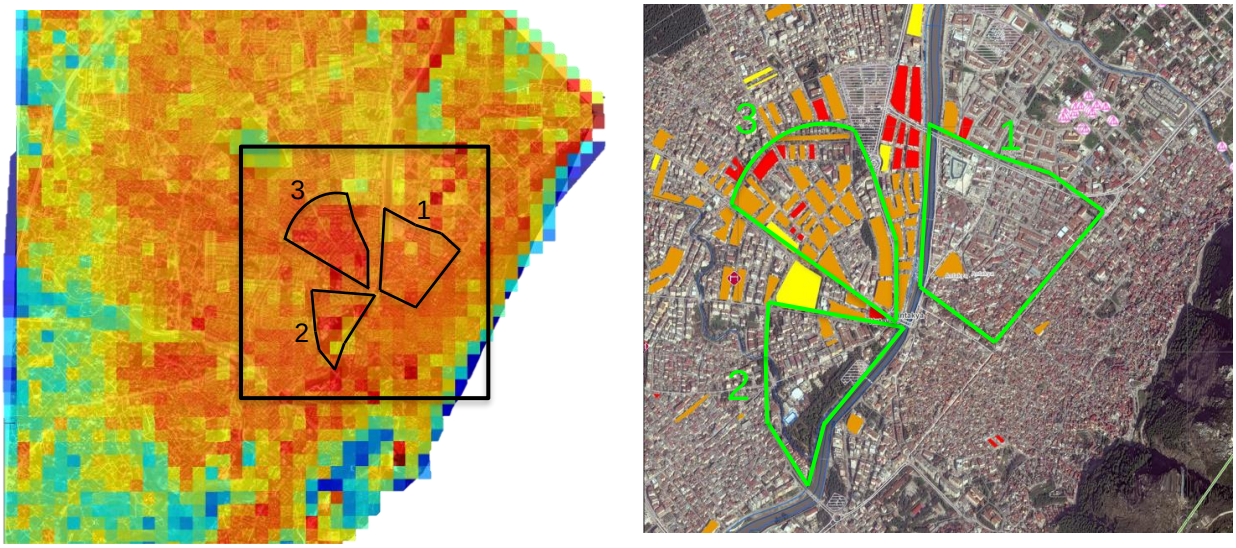

a) b)

Figure 3. Visual comparison of damage grade assessment on same spatial resolution VHR images using a) CVA method and b) Published report by Copernicus (2023) on city of Antakya. (The selected Areas of Interest (AoIs) are identical to provide examples for comparison)

*Description: Legend for b) Copernicus (2023)

Destroyed	Damaged	Possibly damaged

Based on the evaluated results from all five rapid response damage assessment methods, the CVA approach appears to be more compatible with the outcomes of the EMS-98 criteria-based framework, especially in the identification of damage levels within defined patches.

Given the utilization of the same Very High Resolution (VHR) satellite images from Copernicus (2023) for rapid damage assessment in the area, the application of the CVA method in this study enabled the detection of a wider range of possible damages throughout the entire city of Antakya, with a more detailed classification of the damages. Figure 3 visualizes the comparison between the results published by Copernicus (2023) and the utilization of the CVA algorithm on Areas of Interest (AoIs) in a selected zone within the city of Antakya.

5. VHR satellite image diagnosis and SERAMAR prognosis

In a study by Hasan *et al.* (2023), the macroseismic intensity assessment following the 2023 earthquake in Turkey was evaluated using the concept of cumulative cascading events. This was due to the impacts of two major tremors affecting extensive overlapping areas. Based on the latest version of time-dependent SHAKE-

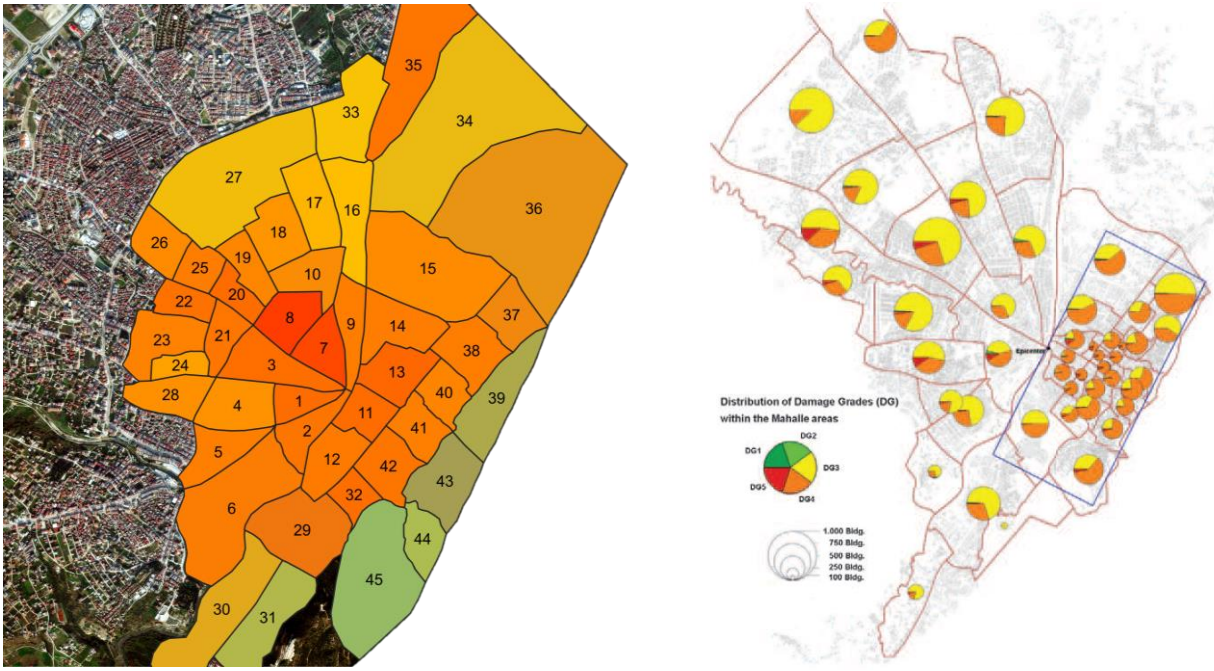

a) b)

*Description: Legend for a) and b)

Legend	< 0.4	0.4 - 0.5	0.5 - 0.6	0.6 - 0.7	0.7- 0.8	0.8 - 0.85	0.85 <
$D_{a)}$	*No DG*	*Less DG*	*Few DG*	*Moderate DG*	*High DG*	*Very high DG*	*Total DG*
$D_{EMS-98,a)}$	*0*	*0 < Di ≤ 1*	*1 < Di ≤ 2*	*2 < Di ≤ 3*	*3 < Di ≤ 4*	*4 < Di ≤ 5*	*5*
$DG_{b)}$	*1*	*2*	*3*	*4*	*5*		

Figure 4. Visual comparison of average damage grades in districts between a) rapid response diagnosis using VHR satellite images and b) prognosis of scenarios designed in the SERAMAR project for I=X.

map development from this study, the final calculated intensity for Antakya is rated IX-X. This aligns closely with one of the intensity levels defined for this area in the SERAMAR project provided by Schwarz et. al. (2012). Due to the absence of quantitative data for the SERAMAR project, the results of one scenario executed by I=X have been visually compared. This comparison seeks to assess the compatibility level between the prognosis of the SERAMAR project and the diagnosis derived from VHR satellite images, as shown in Figure 4. It should also be noted that district borders in the SERAMAR project are defined differently than in Schwarz *et al. (*2008). Additionally, the portion of EMS-98 damage grades is represented by pie charts for each district.

Considering the average damage grades represented by pie charts for districts in the SERAMAR project, the following results can be deduced:

1. For districts outside the rectangular zone, the mean damage grade values fall within 3 ≤ Di ≤ 4. These values are generally comparable to the results from the CVA-rapid response method, with the exceptions of districts 7 and 8.

2. Within the rectangular zone, pie charts indicating mean damage grade values of 4 ≤ Di ≤ 5 align closely with districts 11 and 13. Districts with lower average damage grades show good compatibility with the results of the CVA method derived from VHR satellite images.

6. Conclusion

To assess the compatibility of damage grade evaluations following the cascading earthquakes on 6th February 2023 in Antakya, two temporal VHR satellite images were utilized. The results were then compared with the

outcomes of the SERAMAR project's designed scenarios using both rapid response methods and the EMS-98 criteria-based framework.

Given the strong alignment of the CVA method with visual damage assessment using the criteria-based framework, the results of the CVA approach were used to assess the SERAMAR project's scenarios at a comparable macroseismic intensity level. This analysis revealed a reasonable compatibility between the prognosis of the SERAMAR project and the diagnosis derived from VHR satellite images.

Using the outcomes of the EMS-98 criteria-based framework as a reference, the CVA, combined discriminant, and image difference methods demonstrated the best fit in descending order of accuracy among the examined rapid response methodologies for VHR satellite images, respectively.

7. References

Çetin K., Ilgaç. M. (2023). Reconnaissance report on February 6, 2023 Kahramanmaraş-Pazarcık (Mw=7.7) and Elbistan (Mw=7.6) Earthquakes. *Proceedings of scientific sessions for Türkiye Earthquake Reconnaissance and Research Alliance.*

Copernicus (2023). *Published report on http://emergency.copernicus.eu/mapping/ems/cite-copernicus-ems-mapping-portal.*

Grünthal, G. (ed.), Musson, R., Schwarz, J., Stucchi, M. (1998): European Macroseismic Scale 1998 (EMS-98). *Cahiers du Centre Européen de Geodynamique et de Seismologie,* Volume 15, Luxembourg 1998.

Hadidian, N., Schwarz, J. (2022). EMS-98 based damage grade assessment using remote sensing images for cascading events*, 3ECEES conference,* Bucharest, Romania*.*

Hadidian, N., Schwarz, J. (2023). Building damage assessment for 2021 flood event in Germany using airborne and ground based evaluation tools*, IUGG 2023 conference,* Berlin, Germany.

Hasan, P. L., Beinersdorf, S., Schwarz, J. (2023). Reliability of SHAKEmaps for rapid response decisions - as a question of time and generation procedure. *In: Wuttke, F., Aji, H. D. B., Özarmut, A. (eds), 18th D-A-CH Conference on Earthquake Engineering and Structural Dynamics, 14-15 September 2023*. Kiel, Germany, pp. 151–160.

Schwarz J., Langhammer T., Leipold M., Abrahamczyk L., Kaufmann Ch., Lang D.H., Riedel S. (2008): Bewertung der Erdbebenverletzbarkeit eines Gebäudebestandes in innerstädtischen Großräumen – Phase 1 des SERAMAR Projektes. *Bauingenieur 83 – D-A-CH Mitteilungsblatt*.

Schwarz, J., Abrahamczyk, L., Langhammer, T., Leipold, M., Genes, M.C., Bikçe, M., Kaçin, S. (2009): Building typology for risk assessment: case study Antakya (Hatay). *In Proceedings Earthquake & Tsunami 2009,* Istanbul, Turkey.

Schwarz, J., Abrahamczyk, L., Gülkan, P. (2012): SERAMAR – Seismic Risk Assessment and Mitigation in the Antakya-Maras Region on the basis of Microzonation, Vulnerability and Preparedness Studies. *Special Session 25.1 "Findings of the SERAMAR Project" at the 15th World Conference on Earthquake Engineering*, Lisbon, Portugal.

Schwarz, J., Abrahamczyk, L., Hadidian, N., Haweyou, M., Kaufmann, Ch. (2021). Report on Knowledge-based exposure modelling framework depending on the accuracy and completeness of available data. *Version 1.0, Deliverable D4.1. TURNkey project. H2020-SC5-2018.*

SERAMAR project, Earthquake Damage Analysis Center-EDAC (2023). *https://edac.biz/projekte/seramar*

USGS (2023). Earthquake Catalog*. https://earthquake.usgs.gov/earthquakes/search/*